BNL-211823-2019-JAAM

Mo6S8-Based Single-Metal-Atom Catalysts for Direct Methane to Methanol Conversion

H. Zhang, P. Liu

To be published in "Journal of Chemical Physics"

July 2019

Chemistry Department

Brookhaven National Laboratory

U.S. Department of Energy

USDOE Office of Science (SC), Basic Energy Sciences (BES) (SC-22)

DISCLAIMER

Mo_6S_8-Based Single-Metal-Atom Catalysts for Direct Methane to Methanol Conversion

Hao-Tian Zhang[1], *Cheng Liu*[2], *Ping Liu*[3*], *Yun Hang Hu*[1*]

[1] Department of Materials Science and Engineering, Michigan Technological University, 1400 Townsend Drive, Houghton, Michigan 49931-1295, United States

[2] Mechanical Engineering college, Yangzhou University, 196 Huayang West road, Yangzhou, Jiangsu 225127, P. R. China

[3] Chemistry Department, Brookhaven National Laboratory, Upton, New York 11973, United States

Keywords: single-atom catalyst, methane reforming, methanol synthesis, molybdenum sulfide, DFT

Corresponding Author

* Email: pingliu3@bnl.gov ; yunhangh@mtu.edu.

Abstract: The single atom catalysts have been attracting much attention for catalysis. In this work, the significant influence of single-metal-atom (M = K, Ti, Fe, Co, Ni, Cu, Rh) doping on a Mo_6S_8 cluster was revealed for the direct methane to methanol conversion in water stream using density functional theory (DFT) calculations. It was found that all single atom dopants help to facilitate the conversion via the SRM. The single Fe atom on Mo_6S_8 (Fe-Mo_6S_8) exhibits the most significant promoting effect, which is followed by Ni, Co, Rh-Mo_6S_8 > K, Ti, Cu-Mo_6S_8 > Mo_6S_8 in a decreasing sequence. The enhanced activity by single atom doping on Mo_6S_8 is mainly associated with the interplay between the ensemble effect via the direct participation of active M dopant and the site confinement imposed by doping of single M atom, in tuning the methane conversion and methanol selectivity. It generates the new active center, M, which confines the SRM to occur at the bridge between M and neighboring Mo sites and facilitates the selective production of methanol. A good single-atom promoter should not only bind *OH or *O moderately, being strongly enough to help water dissociation and weakly enough to allow the oxidation of methane, but also impose confinement effect to facilitate the C-O bond association and production of methanol. Our results highlight the importance of the interplay among ligand, ensemble and confinement effects in promoting the complex SRM over single atom catalysts.

1. Introduction

Methane (CH_4) is the main component of natural gas and also a greenhouse gas.[1,2] It is one of the most important research areas to convert CH_4 into value-added chemicals, such as syngas (H_2/CO),[3] formaldehyde,[4] and hydrogen.[5] The direct synthesis of methanol (CH_3OH) from CH_4 has attracted considerable attentions.[6-20] First of all, CH_3OH is currently considered one of the most useful chemical products and is a promising building block for obtaining more complex chemical compounds, such as acetic acid, dimethyl ether, methylamine, etc.. Secondly, the direct $CH_4 \rightarrow CH_3OH$ is more economical and environmentally friendly than the multiple steps process. For the time being, the dominant method of producing CH_3OH is a two-step process. The first step is the conversion of CH_4 into syngas ($H_2O + CH_4 \rightarrow CO + 3H_2$). This step is very energy intensive and represents the major expense in CH_3OH production. The second step is the reaction of the syngas to selectively produce CH_3OH. The direct method can eliminate the need for expensive steam reforming, reducing the number of stages, and thus avoiding the large capital investment required to build a syngas industrial plant. However, the current catalysts are not viable and suffer the low CH_4 conversion and/or low CH_3OH selectivity.[21]

Methane monooxygenase (MMO) in methanotropic bacteria is a highly selective $CH_4 \rightarrow CH_3OH$ catalyst in nature,[22] where a di-Fe or a di-/tri-Cu core was found to be the active center. Although the MMO works well in natural environment, it suffers from a limited stability range with respect to numerous environmental parameters and are not practical for industrial-scale reactions. Inspired by these prototypical natural machines, the metal-exchanged zeolites catalysts, e.g. Cu-exchanged mordenite zeolite[8] and highly dispersed CuO on SBA-15[23], have been extensively studied to mimic the active center of MMO. However, the conversion of CH_4 over the zeolite-based catalysts are still too low for practical application. Thus, the development of practical

catalysts with the high CH_4 conversion and CH_3OH selectivity becomes more and more imperative.

A good catalyst for direct $CH_4 \rightarrow CH_3OH$ should operate under relatively mild conditions, being able to activate the C-H bond of CH_4, but still enabling the formation of CH_3OH. It is very challenging to meet both criteria, which operate in an opposite direction. Besides, the desired product, CH_3OH, is less stable than CH_4, which easily results in over-oxidations into formic acid or carbon oxides.[24] Another challenge is the stability of catalysts, in which coking has been observed due to the strongly adsorbed carbon (*C) or other carbon-related species from the decomposition of CH_4.[25] Here we employ density functional theory (DFT) to study the direct $CH_4 \rightarrow CH_3OH$ conversion in water stream or steam reforming of methane (SRM: $CH_4 + H_2O \rightarrow CH_3OH + H_2$), which acts as operating agent to oxidize CH_4 to CH_3OH according to our previous study on metal oxides.[19]

Moving from metal oxides, the interest in this study for the SRM is molybdenum sulfide (MoS_x), specifically Mo_6S_8 model clusters modified by the singly-doped metal atom (M = K, Ti, Fe, Co, Ni, Cu, Rh). In recent years, single-atom catalysts (SAC) have attracted boosting attention, where the singly dispersed metal atom can be expected for higher selectivity and activity due to the imposed site confinement and improved atomic efficiency.[26,27] In terms of CH_4 activations, the SAC Pd_1, $Pt_1/CeO_2(111)$,[28,29] $Pt_1/Cu(111)$,[30] $Rh/12CeO_2\text{-}Al_2O_3$,[31] Fe/SiO_2,[32] Ni/MgO,[33] and Co/graphene[34] have been reported, being able to promote the activity, alcohol selectivity, or coking resistance. The MoS_x-based SACs are mostly based on the Mo_6S_8 model cluster, a structural block in Chevrel phase of MoS_x. Previously, Mo_6S_8 has been reported to show higher CH_3OH selectivity than MoS_2 bulk, which produces only hydrocarbons and CO_2 from syngas.[35,36] According to the DFT calculations, the synergy between Mo and S via the unique structure of

Mo_6S_8 can prevent the C-O bond cleavage of H_xCO intermediates that was observed on MoS_2 bulk, which eventually hinders the methanation reaction and tunes the selectivity toward to CH_3OH.[37] The later DFT study predicted that the activity and selectivity of Mo_6S_8 can be tuned toward CH_3OH by the singly doped K atom,[38] toward ethanol (C_2H_5OH) by the singly doped Ni atom, and toward CO by the singly doped Pd or Rh atom during CO_2 hydrogenation.[39-41] In contrast, little has been reported for CH_4 activation on Mo_6S_8-based catalysts. To the best of my knowledge, CH_4 activation on Mo_6S_8-based catalysts has not yet been explored theoretically or experimentally. The present DFT calculations show that the single-atom dopants (M = K, Ti, Fe, Co, Ni, Cu, Rh) studied help in accelerating H_2O dissociation and providing active *OH or *O species to facilitate the C-H bond cleavage of CH_4 and thus the CH_3OH formation. The origin of promoting effect introduced by doped single-metal-atom on Mo_6S_8 is associated with the synergy among the ligand effect via the electronic modification on M-Mo_6S_8 interaction, ensemble effect via the direct participation of M dopants and the confinement effect via the reforming reaction limited to occur only over the neighboring $Mo^{\delta+}$ and $M^{\delta+}$ sites.

2. Computational Method

Spin-unrestricted DFT calculations for the activation and conversion of CH_4 and H_2O to CH_3OH on a M−Mo_6S_8 cluster were performed with the projector-augmented-wave[42] method using the Vienna ab initio simulation package (VASP)[43,44] and GGA-PBE[45] for the exchange and correlation functional. The kinetic energy cutoff for a plane wave basis set was 500 eV. Only Γ-points was considered for the calculations. M−Mo_6S_8 clusters were allowed fully relaxed together with the adsorbates. Relaxations of the ion positions were performed using a conjugate gradient algorithm, until the forces on all atoms were less than 0.01 eV/Å and convergence to 1E-5 eV of

the total electronic energy. The Mo-S bond length is 2.46 Å which is in a good agreement with previous work.[37,38] The calculated adsorption energy was expressed as E_{ads} = E (adsorbate/Cluster) - E (Cluster) - E (adsorbate), where E (adsorbate/Cluster), E (Cluster) and E (adsorbate) represent the total energies of Mo_6S_8 interacted with the adsorbate, Mo_6S_8 cluster in gas phase and the adsorbate in gas phase, respectively. The transition states were located by Nudged Elastic Band (NEB) method and confirmed with frequency calculations.[46-51]

3. Result and Discussion

3.1. Geometry and stability of M-Mo_6S_8 cluster

The stability of Mo_6S_8 cluster is firstly studied. Each S atom tightly combines with three Mo atoms and a binding energy of -5.90 eV. This strong interaction can prevent the decomposition of Mo_6S_8 cluster in the reaction environment. Also, the oxidation of Mo_6S_8 cluster is energetically unfavorable. The replace of S atom by O atom is extremely endothermic with a reaction energy of 4.06 eV, indicating that the Mo_6S_8 likely survives under oxidizing environment. Indeed, as will be seen below, the Mo_6 core of Mo_6S_8 cluster remains intact in interaction with various reaction intermediates, though it distorts. Thus, the Mo_6S_8 structural motif is likely maintained during the SRM due to strong binding between S and Mo atoms.

According to our DFT calculations, the singly doped M (M = Ti, Fe, Co, Ni, Cu, Rh) can be well stabilized at the S-Mo-Mo-S 4-fold sites at the edge of Mo_6S_8 cluster (Figure 1a), or (M = K) at the S-S 2-fold site (Figure 1b), which are accompanied with the oxidation of M and reduction of neighboring Mo via the emergence of new Mo 4d intermediate states at the Fermi level (Figure 2). This is in a good agreement with the previous studies.[38-41] The binding energy of M and Mo_6S_8 follows the order: Ti > Rh > Fe > Ni > Co > K > Cu (Table 1). The interaction between early transition metal, Ti, and Mo_6S_8 cluster is the strongest (E_{ads} = -5.24 eV) among all evaluated

systems, while the noble metal, Cu, corresponds to the weakest interaction (E_{ads} = -2.55 eV). The alkali metal, K, loses the one electron and forms K^+ on interaction with Mo_6S_8, with no contribution near the Fermi level (Figure 2). However, due to the electrostatic repulsion between K^+ cation and $Mo^{\delta+}$, only the 2-fold S-S site is observed, and the corresponding interaction is just slightly stronger (E_{ads} = -2.71 eV) compared to Cu-Mo_6S_8, in consistent with our previous study.[38] More importantly, although the M-Mo_6S_8 interaction is strong, the Mo_6 octahedral core remains mostly intact with slight structural distortion. That is, the cage structure of Mo_6S_8 is stable enough to survive in interaction with the active dopants.

3.2. Methane Adsorption and Dissociation

On Mo_6S_8, the stable adsorption of CH_4 is at the Mo top site (E_{ads} = -0.30 eV, Figures 3 and 4). The doping of single-metal-atom does not affect the bonding motif via H of CH_4, which was previously proposed as the precursor for CH_4 activation,[52] while it varies the interaction with CH_4, via either ligand effect (the modification of electronic structure of $M^{\delta+}$ and $Mo^{\delta+}$) or the ensemble effect (the direct participation of M in binding). The E_{ads} of CH_4 decreases in the order: Ni-Mo_6S_8 > Co-Mo_6S_8 > Ti-Mo_6S_8 > Fe-, Cu-Mo_6S_8 > Mo_6S_8 > K-Mo_6S_8 > Rh-Mo_6S_8 (Table 2). In term of ligand effect, the CH_4-Mo interaction on Mo_6S_8 can be further weakened by doping single-metal-atom (M = K, Ti, Fe, Co, Ni, Cu, Rh, Table 2), which is associated with the electrostatic repulsion between H^+ of CH_4 and the doped single $M^{\delta+}$ via the M→Mo_6S_8 electron transfer (Figure 2). It prevents the approaching of CH_4 molecule toward the cluster. Such repulsion is particularly significant for fully oxidized K^+. Nevertheless, the Mo top site of K-Mo_6S_8 is the most stable site for CH_4 due to the inertness of K^+ (Figure 3). By comparison for M-Mo_6S_8 (M = Ti, Fe, Co, Ni, Cu), M is less oxidized (Figure 2). In these cases, $M^{\delta+}$ is active enough to stabilize

CH_4 (Table 2), where the ensemble effect plays a significant role and the M rather than Mo top site is preferred (Figure 3). Nevertheless, the effect of doping single-metal-atom on the adsorption of CH_4 is rather small and the corresponding bindings on all systems studied are relatively weak (Table 2). The most promotion in binding is by doping Ni on going from -0.30 eV for Mo_6S_8 to -0.53 eV for Ni-Mo_6S_8. Rh is the only 4d metal dopant considered in our study. Compared to the 3d metal dopants, Rh is the least oxidized;[38] however, with the lower-lying d-band (Figure 2) the doped single Rh atom is not active enough to adsorb CH_4 according to the d-band theory,[53] and the molecule still favors the Mo top site as the cases of K-Mo_6S_8 and Mo_6S_8 (Table 2). However, the Rh sites are highly active to stabilize the dissociated fragments from CH_4 and H_2O as will be shown in the following.

The CH_4 dissociations on all studied clusters are highly endothermic process (Figure 4). The undoped Mo_6S_8 cluster displays the higher endothermicity than M-Mo_6S_8 clusters, where the energy is uphill all the way going from *CH_4 (-0.30 eV) to *C (3.68 eV). The hydrogen abstraction proceeds at the Mo-S hybrid sites (Figure 3). The first C-H bond cleavage (*CH_4 + * $\rightarrow$ *CH_3 + *H) corresponds to an energy barrier (E_a) of 1.45 eV (Figure 4), while E_a for the second (E_a = 1.07 eV, *CH_3 + * $\rightarrow$ *CH_2 + *H) and the third (E_a = 1.17 eV, *CH_2 + * $\rightarrow$ *CH + *H) is slightly lower. The most difficult step, though, is the formation of *C (*CH + * $\rightarrow$ *C + *H) with E_a as high as 2.00 eV. It means that the coking can be greatly hindered on Mo_6S_8 when exposure to CH_4. During the dissociation, the S atom also helps to facilitate the C-H bond cleavage via the stabilization of the dissociated *H atom (Figure 3), which was also observed previously for hydrogenation reactions.[38-41] Here, we note that the effect of coadsorption of *H on the energetics was not included in the potential energy diagram. In agreement with our previous studies on Mo_6S_8 and doped- Mo_6S_8,[37,38] the present calculation show that *H prefers to the S site via the strong S-H

bond and does not compete with the other intermediates for the active sites (Mo or M). In addition, the binding energy does not vary significantly on coadsorption with other intermediates (< 0.2 eV) and the shift in energy in potential energy diagram by including coadsorbed *H remains mostly the same. In addition, the high mobility of *H under the methane activation conditions likely enables the facile recombination of two *H and desorption.

The single-metal-atom dopants display more significant effects on the hydrogen abstraction of CH_4 as compared to the molecular adsorption. For the first hydrogen abstraction, the corresponding E_a decreases in the order: Co-Mo_6S_8 (E_a = 0.58 eV) > Fe-Mo_6S_8 (E_a = 0.71 eV) > Ti-Mo_6S_8 (E_a = 0.83 eV) > Ni-Mo_6S_8 (E_a = 1.07 eV) > K-Mo_6S_8 (E_a = 1.33 eV) > Mo_6S_8 > Rh-Mo_6S_8 (E_a = 1.51 eV) > Cu-Mo_6S_8 (E_a = 1.72 eV). The doping of single-metal-atom of Co, Fe, Ti, and Ni greatly lowers the reaction energy and the corresponding barrier for the first hydrogen abstraction on Mo_6S_8. The ensemble effect plays a dominant role in these cases, as demonstrated by the direct participation of doped $M^{\delta+}$ in stabilizing *CH_4 and the dissociated *H (Figure 3). The higher activity of single-metal-atom $M^{\delta+}$ (M = Co, Fe, Ti, Ni) than $Mo^{\delta+}$ is associated with the lower oxidation state. The corresponding d states of $M^{\delta+}$ locate closer to the Fermi level than that of $Mo^{\delta+}$ (Figure 2), which helps to thus stabilize the reaction intermediates (*CH_4, *CH_3 and *H) and the transition states via the facilitated electron transfer from the cluster. Here we note that the first C-H bond cleavage of *CH_4 at the Fe site of Fe-Mo_6S_8 is lower in E_a by 0.95 eV than that of Fe-based sMMO catalyst,[54] while it is higher by ~0.2 eV than that of Fe-ZSM due to the assistance of O atom from the confined envronment.[55,56] In contrast, the ensemble effect introduced by doping Cu is opposite. The dehydrogenation of *CH_4 on Cu-Mo_6S_8 corresponds to the highest barrier among all the systems studied. In this case, the doped Cu corresponds to the lower-lying d states than the other dopants (Figure 2), which hinders the stabilization of transition state for C-H bond

cleavage, specifically *H, and thus raises the activation barrier. Similarly, the doping of Rh also does not help for the first hydrogen abstraction, though the Rh site directly participates in interaction with the dissociated $*CH_3$ via the ensemble effect. The corresponding barrier on Rh-Mo_6S_8 is 0.21 eV lower than that of Cu-Mo_6S_8. This is due to the less stable initial state, $*CH_4$, introduced by doping Rh than Cu (Figure 4). With one electron transfer, K^+ on Mo_6S_8 does not contribute to the states near the Fermi level, while the donated electron results in the reduction of $Mo^{\delta+}$ is observed with some of the low empty states of Mo 4d states filled (Figure 2). The reduction of Mo is supposed to help the adsorption of CH_4, while the binding on K-Mo_6S_8 is weaker than Mo_6S_8 due to the dominating electrostatic H^+-K^+ repulsion (Table 2). Yet, the transition state for the C-H cleavage on K-Mo_6S_8 is energetically comparable to that of Mo_6S_8 (Figure 4), as the destabilization of $*CH_3$ due to electrostatic repulsion is compensated by the stabilization of dissociated *H by reduced $Mo^{\delta+}$ at the transition stage (Figure 3). As a result, the overall barrier is slightly lowered.

The single-metal-atom dopants cause the difficulty for the second hydrogen abstraction, where the corresponding barrier increases following the order of Mo_6S_8 < Rh-Mo_6S_8 (E_a = 1.21eV), K-Mo_6S_8 (E_a = 1.24 eV) < Co-Mo_6S_8 (E_a = 1.35 eV), Ti-Mo_6S_8 (E_a = 1.33 eV) < Cu-Mo_6S_8 (E_a = 1.49 eV) < Ni-Mo_6S_8 (E_a = 1. 65 eV) < Fe-Mo_6S_8 (E_a = 1.83 eV). For M = Co, Fe, Ti, Ni, Rh, Cu, the direct participation of doped single M atom in binding (Figure 3) particularly promotes the stability of $*CH_3$ as compared to Mo_6S_8 (Figure 4), which hinders the dissociation. That is, the ensemble effect of single-metal-atom dopants suppresses the $*CH_3$ dissociation, whereas the ligand effect is rather weak. In the case of K-Mo_6S_8, the H^+-K^+ electrostatic repulsion drives the adsorption of $*CH_2$ away from K^+ (Figure 4) toward the dissociated *H. As a result, the $*CH_3 \rightarrow$

*CH_2 transition state is destabilized due to lateral repulsion. During this process, K^+ is not directly involved.

The barrier for *CH_2 dissociation to *CH increases in the order of Ni-Mo_6S_8 (E_a = 0.47 eV) < Fe- (E_a = 0.69 eV), Co-Mo_6S_8 (E_a = 0.69 eV) < Mo_6S_8 (E_a = 1.17 eV), K-Mo_6S_8 (E_a = 1.18 eV) < Cu-Mo_6S_8 (E_a = 1.30 eV) < Rh-Mo_6S_8 (E_a = 1.46 eV) < Ti-Mo_6S_8 (E_a = 1.77 eV). Ti-Mo_6S_8 displays the highest barrier toward *CH_2 dissociation; while the introduction of Fe, Co, or Ni single-atom can accelerate the process on Mo_6S_8 (Figure 4). Again, the ensemble effect induced by the doped M makes the dominant contribution to tune the energetics (Figure 3). K-Mo_6S_8 is the only exception, where only the ligand effect matters.

The barrier for *CH dissociation to *C increases in the order of Co- Mo_6S_8 (E_a = 0.99 eV), Ni-Mo_6S_8 (E_a = 1.00 eV) < Fe-Mo_6S_8 (E_a = 1.14 eV) < Cu-Mo_6S_8 (E_a = 1.31 eV) < K-Mo_6S_8 (E_a = 1.51 eV) < Rh-Mo_6S_8 (E_a = 1.66 eV) < Ti-Mo_6S_8 (E_a = 1.82 eV) < Mo_6S_8 (E_a = 2.00 eV). The adsorption of *CH is comparable on the clusters with and without doping, whereas the final dissociation state, *C, can be significantly stabilized on M-Mo_6S_8 (Figure 4), where *C adsorbs at hollow sites for all clusters, and forms the strong binding with S, Mo and M atoms (Figure 3). The facilitated *CH dissociation is associated with the formation of strong M-C bond via the ensemble effect (Figure 3). In the case of K-Mo_6S_8, the enhancement solely depends on the ligand effect. The reduced $Mo^{\delta+}$ by K doping helps to strengthen the Mo-CH binding as compared to Mo_6S_8, while the weakening due to the H^+-K^+ electrostatic repulsion is less significant.

The doping of single-metal-atom significantly influences the CH_4 adsorption and dissociation on Mo_6S_8. The ensemble effect plays a dominating role in strengthening the binding and lowering the barriers via direct binding with *CH_x for M = Co, Ni, Cu, Rh, Fe, Ti. In contrast, only the ligand effect matters for the case of K-Mo_6S_8, where the doped K^+ is involved in the

reaction indirectly via the electron transfer from K to Mo_6S_8 and the reduction of $Mo^{\delta+}$. The step corresponding to the highest barrier varies depending on the dopant. For M= K, Rh, and Ti, the *CH → *C transition remains as the most difficult step as that of Mo_6S_8, while it is $*CH_3 \rightarrow *CH_2$ for M = Fe, Ni, Co and $*CH_4 \rightarrow *CH_3$ for M=Cu (arrow, Figure 4). According to the highest barrier along the pathway, the Co-Mo_6S_8 is likely the most effective catalyst among all the examined clusters, which is followed by Mo_6S_8 > K-Mo_6S_8 > Ni-, Rh-Mo_6S_8 > Ti-Mo_6S_8 > Cu-Mo_6S_8 > Fe-Mo_6S_8 in a decreasing sequence (Figure 4). Furthermore, the suppression of $*CH_3$ dissociation on Mo_6S_8 introduced by for doping (M = Fe, Ni, Co) can be beneficial for the direct CH_3OH synthesis, being able to selectively increase the $*CH_3$ species and thus facilitate the $*CH_3 \rightarrow *CH_3OH$, but also hinder the undesired syngas formation and carbon deposition.

3.3. H_2O Adsorption and Dissociation

During the SRM reaction, H_2O may compete with CH_4 for the same kind of active sites on Mo_6S_8 and M-Mo_6S_8 clusters. Indeed, as the case of CH_4, H_2O also prefers the Mo top site on Mo_6S_8, Rh-Mo_6S_8 and K-Mo_6S_8, whereas the adsorption favors M top sites for Ti-, Fe-, Co-, Ni-, and Cu-Mo_6S_8 clusters (Figure 5 and Table 3). The adsorption of $*H_2O$ on the Mo_6S_8 is more favorable (E_{ads} = -0.83 eV, Table 3), which is comparable to that of bulk MoS_2.[57] By doping the single-metal-atom (M = K, Cu, Fe, Ni, Co, Ti), the $*H_2O$ adsorption is enhanced by 0.05 eV, 0.05 eV, 0.09 eV, 0.14 eV, 0.16eV, and 0.19 eV on Mo_6S_8, respectively (Table 3). On K-Mo_6S_8, the enhancement in $*H_2O$ adsorption is contributed by both ligand and ensemble effects. Wherein, the ligand effect promotes the Mo-OH_2 interaction via the reduced $Mo^{\delta+}$ as the case of *CH, while different from $*CH_4$ or $*CH_3$ adsorption the ensemble effect stabilizes $*H_2O$ via the O^{2-}-K^+ electrostatic attraction (Figure 5). For M = Ti, Fe, Co, Ni, Cu, the stabilization of $*H_2O$ is due to

the higher lying d states of the doped $M^{\delta+}$ than $Mo^{\delta+}$ (Figure 2), which favors the direct M-O bond formation and thus the adsorption enhancement via the ensemble effect. Rh-Mo_6S_8 behaves similarly as that of Mo_6S_8. The adsorption at Mo top remains as the most stable (ligand effect) with the $Rh^{\delta+}$ shifts away from *H_2O (Figure 4). Yet, the adsorption on the Rh site (ensemble effect) is comparable with only 0.01 eV less stable than that on that Mo site (Table 3) and the corresponding interaction is weakened by only 0.04 eV as compared to Mo_6S_8.

The *H_2O dissociation on Mo_6S_8 occurs over the Mo-S hybrid site, where Mo and S atoms help to stabilize the dissociated *OH and *H, respectively (Figure 5). Similar motif is observed for the *OH dissociation, where the dissociated *O prefers the Mo top site and introduces significant structural distortion of Mo_6S_8 (Figure 5). Energetically (Figure 6), the first hydrogen abstraction to *OH and *H is less favorable (E_a = 1.22 eV) than that on bulk MoS_2 surface (E_a = 1.01 eV).[57] While the second abstraction is greatly facilitated on Mo_6S_8 (E_a = 1.21 eV) as compared to that of MoS_2 (E_a = 1.93 eV).[57] This is due to fact that the unique Mo_6S_8 structure enables the formation of Mo=O oxo species to promote the stability of the dissociated *O (Figure 5).

The formation of M-Mo_6S_8 promotes the *H_2O dissociation to *OH with the barrier decreasing in the order of Mo_6S_8 (E_a = 1.22 eV) > Ni-Mo_6S_8 (E_a = 1.10 eV) > Cu- (E_a = 1.01 eV), Rh-Mo_6S_8 (E_a = 1.03 eV) > Co-Mo_6S_8 (E_a = 0.99 eV) > K-Mo_6S_8 (E_a = 0.66 eV) > Ti-Mo_6S_8 (E_a = 0.45 eV) > Fe-Mo_6S_8 (E_a = 0.42 eV) (Figure 6). The promotion is mostly via the ensemble effect, where the dopant enables the stabilization of the dissociated *OH by shifting the adsorption site from the M atop site to the Mo-M bridge site (Figures 5 and 6). The Rh-Mo_6S_8 and K-Mo_6S_8 behave slightly different. For Rh-Mo_6S_8, the favorable site varies from the Mo top for *H_2O to the Rh top site for *OH (Figure 5), while in the case of K-Mo_6S_8 the preference to the K-Mo sites remains during the dissociation. The drawback is, though, the stabilized *OH on the M-Mo_6S_8

clusters hinders the dissociation of *OH to *O. This is the case for M = Ni (E_a = 1.33 eV), Co (E_a = 1.67 eV), Cu (E_a = 1.73 eV), K (E_a = 1.74 eV), Rh (E_a = 1.80 eV), where the dissociated *O remains or shifts to the Mo-M bridge site (Figures 5 and 6). In contrast, the single Ti (E_a = 1.03 eV) and Fe (E_a = 1.09 eV) dopants help to lower the barrier. This is due to the stronger interaction between $Fe^{\delta+}$/$Ti^{\delta+}$ and the intermediates (*OH and *O) than the other dopants (Figure 6), which results in a lower barrier for the dissociation of *H_2O and *OH. We note, among the systems studied the most significant structural distortion is observed for Cu-Mo_6S_8 during the H_2O dissociation, which breaks Cu-S bonds, weakens the interaction between Cu and Mo_6S_8, and results in the least stable *O adsorption; yet the Mo_6 octahedral core keeps its structure intact (Figures 5 and 6).

In term of adsorption site, CH_4 and H_2O compete for the same active site (Mo or M) on Mo_6S_8 and M-Mo_6S_8 clusters (Figures 3 and 5). Energetically, the *H_2O adsorption is always more favorable than that of *CH_4 (Tables 2 and 3). That is, under the SRM condition the active sites are likely occupied by H_2O first, which is followed by dissociation. The generated *OH or *O species at the active sites can become the new active sites for CH_4 to CH_3OH conversion according to the previous studies.[14,58]

3.4 SRM toward CH_3OH synthesis

The preferential H_2O adsorption and dissociation over CH_4 result in the formation of *O on Mo_6S_8, which is more favorable than the formation of *OH (Figure 6). On the *O-covered Mo_6S_8 cluster, the formed Mo=O oxo group from *H_2O adsorption is too stable to activate CH_4. As shown in Figure 7, the direct CH_4 dissociation to CH_3OH (*O + CH_4 $\rightarrow$ *CH_3OH) is highly activated (E_a = 2.22 eV). By comparison, OH-assisted CH_4 dissociation (*OH + CH_4 $\rightarrow$ *CH_3 +

*H_2O) is more favorable (E_a = 1.20 eV); yet *OH is not as stable as *O on Mo_6S_8 (Figure 6). Previously, the Cu, Fe=O oxo groups were proposed as the active sites for direct $CH_4 \rightarrow CH_3OH$ conversion in MOFs and zeolites with structural confinement.[30,58,59] As shown in Figure 7, the transition structure for $CH_4 \rightarrow CH_3OH$ conversion on the Mo=O of Mo_6S_8 is similar to that of Fe=O of zeolite.[58] However, the rigid octahedral Mo_6 structure hinders the Mo-O interaction and thus the capability in stabilizing CH_4 and H-O$\cdots$$CH_3$ transition state. As a result, the corresponding initial and transition states involved show a longer adsorbate-oxo bond and smaller structural changes in CH_4 (Figure S1) as compared to that of Fe=O in zeolite.[58] That is, the metal-oxo motif is not necessarily the active sites for CH_4 activation, where the fluxionality of local structure can be important. The overall reaction is hindered by the CH_4 dissociation to CH_3OH at *O site, which corresponding the highest barrier of 2.22 eV along the pathway (Figure 7).

Upon going from Mo_6S_8 to Fe-Mo_6S_8, the dissociated *OH from *H_2O occupies the active Fe sites, which is more favorable than the *O formation (Figure 6). The *OH at the Fe-Mo bridge site also helps the first C-H bond cleavage of *CH_4 via the stabilization of the dissociated *H by the formation of *H_2O at the Mo top site. While the dissociated *CH_3 fragment is strongly adsorbed at the top of Fe site (Figure 8). The corresponding barrier (E_a = 0.65 eV) is only slightly lower than that on bare Fe-Mo_6S_8 (E_a = 0.71 eV). Furthermore, the produced *H_2O at the Mo site dissociates to *OH (E_a = 0.42 eV), which is much easier than *CH_3 dissociation to *CH_2 (E_a = 1.83 eV) and provides the active sites for *CH_3OH formation via the combination with *CH_3. Like Mo_6S_8, the formation of *CH_3OH via the C-O bond association corresponds to the highest barrier along the pathway (E_a = 0.68 eV); yet it is much lower due to the promoting of doped single Fe atom. We note that the activation of *CH_4 to *CH_3 is also highly activated on Fe-Mo_6S_8 (TS2, Figure 8), which is only 0.03 eV lower in E_a than the most difficult step.

To quantify the activity, the CH_3OH synthesis from the SRM on M-Mo_6S_8 clusters was estimated with respect to Mo_6S_8 via the Arrhenius equation, $e(-\frac{E_a^{Max}-E_a^{Max,Mo_6S_8}}{RT})$, where E_a^{Max} represents the highest barrier along the optimized reaction pathway and the temperature T is 525 K in our cases (Figure 9). One can clearly see that the Fe is more effective than the other dopants studied. The corresponding reaction rate is ~10^{14} times faster than that of Mo_6S_8, which is also higher than extensively studied FeO^+-based catalyst.[54] That is, Fe-Mo_6S_8 can be a promising catalyst for CH_3OH synthesis from CH_4 and H_2O. The highly active single-metal-Fe site constrains *CH_3 and *OH close enough (confinement effect), which enables the stabilization of transition state and thus facilitates the most difficult C-O bond association to produce CH_3OH (TS4, Figure 8). In contrast, the lacking confinement effect in the case of Mo_6S_8 limits the co-adsorption of *O and *CH_x in a neighboring position, and the transition state for C-O bond association involves an unstable -CH_3 radical (TS4, Figure 7). Thus, a higher barrier and lower activity for CH_3OH production on Mo_6S_8 is observed than that on Fe-Mo_6S_8.

The Co, Rh, or Ni dopants also help, though the enhancement is not as significant as that of Fe by ~10^5 in term of reaction rate (Figure 9). The SRM to CH_3OH over Co, Rh, Ni-Mo_6S_8 clusters follows the same pathway as that on Fe-Mo_6S_8 (Figures S2-S4). Differently, *H_2O dissociation to *OH is the step with the highest barrier on Ni-Mo_6S_8 (TS1, E_a = 1.10 eV, Figure S4). It moves to the first C-H bond breaking of *CH_4 in the cases of Co-Mo_6S_8 (TS2, E_a = 1.18 eV, Figure S2) and Rh-Mo_6S_8 (TS2, E_a = 1.22 eV, Figure S3), where *OH helps to stabilize the dissociated *H in the form of *H_2O. The promotion on the C-O association to CH_3OH, which is demonstrated by the doped single Fe atom, is also seen for single Co (TS4, E_a = 0.74 eV, Figure S2), Rh (TS4, E_a = 0.20 eV, Figure S3) and Ni (TS4, E_a = 0.15 eV, Figure S4) atoms (site confinement effect). Again,

the $*CH_3$ and *OH species are positioned closely enough over the dopant site to facilitate the difficult C-O bond association and CH_3OH production on Mo_6S_8.

The least enhancement in CH_3OH synthesis from the SRM is observed when doping Ti, Cu, or K over Mo_6S_8, which is lower than that of Fe by a factor ~10^{10} (Figure 9). On Ti, Cu, K-Mo_6S_8, the CH_4 is activated via the *O species from H_2O (Figures S5-S7) as that of Mo_6S_8. Although for M = Ti, Cu, K the formation of *OH is more favorable than *O (Figure 6), the CH_4 dissociation on *OH to $*CH_3$ + $*H_2O$ or $*CH_3OH$ + *H is more activated than the *OH dissociation to *O (1.73 eV vs. 1.82 eV for Cu-Mo_6S_8, 1.74 eV vs. 2.05 eV for K-Mo_6S_8, 1.03 eV vs. 2.49 eV for Ti-Mo_6S_8). The most difficult step toward the CH_3OH synthesis varies from the $*CH_4$ dissociation at the *O site to $*CH_3OH$ for Mo_6S_8 (TS3, E_a=2.22 eV, Figure 7), to $*CH_3O$ hydrogenation to $*CH_3OH$ by doping Ti (TS4, E_a= 1.79 eV, Figure S5), and the *O formation from *OH dissociation by doping Cu (TS2, E_a= 1.73 eV, Figure S6) and K (TS2, E_a= 1.74 eV, Figure S7). Besides, other steps are also involved, which correspond to a barrier only slightly lower than the highest, typically involved $*CH_4$ oxidation by *O to $*CH_3O$ or $*CH_3OH$ (TS3, Figures S5-S7). Nevertheless, one can see that for Ti, Cu, K-Mo_6S_8 the conversion must overcome several steps with very high energy barriers (> 1.70 eV) and thus, a lower activity toward the SRM than Fe-, Co-, and Rh-Mo_6S_8 is observed (Figure 9). Similar to M = Fe, Co, Rh, Ni, the site confinement effect to promote the C-O bond association is also observed for the single atom Ti doped (TS3, E_a = 1.54 eV, Figure S5), while it is not obvious for the less active Cu (TS3, E_a = 1.22 eV, Figure S6) and K (TS3, E_a = 1.53 eV, Figure S7), where the CH_4 approaches to the *O site from gas phase and the C-O bond association occurs via a transition involving an unstable CH_3 radical.

Overall, the $CH_4 \rightarrow CH_3OH$ conversion on the Mo_6S_8 and M-Mo_6S_8 clusters via the SRM reaction, specifically the elementary step with the highest barrier and thus the overall rate, is likely

to be strongly affected by the binding of *OH or *O from H_2O dissociation. To activate water, *OH should be strongly bound. Once the hydroxylated clusters (Fe, Co, Rh, Ni-Mo_6S_8) is formed, the activation of CH_4 is likely controlled by the step involving *OH as the reactant. Wherein, *OH can either assists the $*CH_4 \rightarrow *CH_3$ dissociation indirectly by stabilizing the dissociated *H in the form of water or participates in directly to oxidize $*CH_3$ and form $*CH_3OH$ via the C-O bond association. Similarly, for the oxidized Mo_6S_8 and Ti-Mo_6S_8, where the oxidation steps involving *O are always highly activated. For the oxidized Cu, K-Mo_6S_8 clusters, though, the CH_3OH synthesis can be slowed down by the most difficult *OH dissociation to *O. Thus, the *OH or *O bonding is always involved in the likely rate-controlling steps as reactants or products, which can be an effective descriptor to capture the difference in $CH_4 \rightarrow CH_3OH$ conversion. Indeed, a volcano-like variation between the estimated reaction rate and the *OH adsorption energy is observed (Figure 9). Similar trend is also observed when using the *O binding as the descriptor, as the stability of *O and *OH is correlated (Figure 6).

A good single-atom promoter to the SRM should provide a moderate *OH binding, being strong enough to allow the adsorption and dissociation of H_2O, but weakly enough to enable the oxidation of CH_4 and facial removal of CH_3OH from the Mo_6S_8 cluster (Figure 9). The dopant like Ti is too active for stabilization of *OH or *O, which hinders the CH_4 oxidation, while the dopant like Cu is too inert, which cannot catalyze the H_2O dissociation well. Single-metal-Fe dopant is the best among the systems studied. It optimizes the reaction pathway via the ensemble effect and confinement effect. Compared to Mo_6S_8, the ensemble effect introduced by the doped single-atom Fe, together with the synergy with the neighboring Mo, enhances the H_2O and CH_4 dissociation via the formation of Fe-OH and Fe-CH_3 bonds. In addition, the introduced confinement effect enables the formation of closely packed $*CH_3$ and *OH over the active single-atom Fe, which

enables the stabilization of transition state and thus facilitates the difficult C-O bond association to produce CH_3OH. By contrast, the contribution from ligand effect is rather small.

4. Conclusion

The direct $CH_4 \rightarrow CH_3OH$ conversion via the SRM and over the single-metal-atom (M = K, Ti, Fe, Co, Ni, Cu, Rh) on Mo_6S_8 clusters were explored using DFT. The M-induced variation in structure and energy of reaction intermediates and transition states was found to be associated with the ensemble effect where M participates directly in binding, and the confinement effect where M enables the closely packed co-adsorption motif to facilitate the difficult C-O bond association and CH_3OH production. By contrast, the ligand effect via electron transfer toward Mo_6S_8 cluster is rather small.

For CH_4 dissociation, the suppression of $*CH_3$ dissociation on Mo_6S_8 is observed for all M-Mo_6S_8 clusters studied, which can increase the $*CH_3$ species and benefit the direct CH_3OH synthesis by oxidation of $*CH_3$. While Co-Mo_6S_8 is the only doped system, which exhibits the promotion for complete CH_4 dissociation via the ensemble effect. In the case of H_2O dissociation, compared to bare Mo_6S_8, the first hydrogen abstraction is enhanced by all the single M atom dopants, whereas the second abstraction is mostly suppressed except Ti and Fe. Ti-Mo_6S_8 shows the highest activity toward H_2O dissociation in our study.

All doped single-atom M show the enhancement in CH_3OH synthesis during the SRM on Mo_6S_8, where the promoting effect of Fe is the most significant, which is followed by Ni, Co, Rh-Mo_6S_8 > K, Ti, Cu-Mo_6S_8 in a decreasing sequence. Under the SRM condition, the active Mo or M sites are likely to be occupied by $*H_2O$, which results in the formation of oxidized or hydroxylated clusters. The binding of *OH or *O is identified as the descriptor for the overall

activities. The best single-atom dopant, e.g. Fe, should enable the bond-tuning and the site confinement effect imposed, being able to facilitate *H_2O dissociation and provide active *OH or *O species, but still enabling the facile association of the *CH_3 and *OH fragments to produce CH_3OH.

Supplementary Material

See Supplementary Material for geometries for initial and transition states involved in the direct $CH_4 \rightarrow CH_3OH$ conversion on *O covered Mo_6S_8. Optimal potential energy diagram and geometries for CH_3OH synthesis on Co-, Rh-, Ti-, Ni-, Cu-, and K-Mo_6S_8 cluster.

ACKNOWLEDGMENT

This work was supported by the U.S. Department of Energy (DOE), Office of Science, Office of Basic Energy Sciences, Division of Chemical Sciences, Biosciences and Geosciences, under contract No. DE-SC0012704. The DFT calculations were performed using computational resources at the Center for Functional Nanomaterials, a U.S. DOE Office of Science Facility, and the Scientific Data and Computing Center, a component of the Computational Science Initiative at Brookhaven National Laboratory. Z.H.T. and Y.H.H. would like to thank the support from the U.S. National Science Foundation (CMMI1661699).

REFERENCES

[1] R. W. Howarth, “A bridge to nowhere: methane emissions and the greenhouse gas footprint of natural gas,” Energy Sci. Eng. **2**, 47–60 (2014).

[2] J. Z. Daniel, L. W. Laurie, L. V. Timothy, Q. Casey, R. Subramanian, P. D. Gerald, W. Bryan, D. O. Jean, J. M. Anthony, M. M. David, L. R. Allen, "Methane Emissions from the Natural Gas Transmission and Storage System in the United States," Environ. Sci. Technol. **49**, 9374-9383 (2015).

[3] M. J. D. Silva, "Synthesis of Methanol from Methane: Challenges and Advances on the Multi-Step (Syngas) and One-Step Routes (DMTM)," Fuel Proc. Tech. **145**, 42-61 (2016).

[4] V. Fornés, C. López, H. H. López, A. Martínez, "Catalytic performance of mesoporous VO_x/SBA-15 catalysts for the partial oxidation of methane to formaldehyde," Appl. Catal. A: General, **249**, 345-354 (2003).

[5] H. F.; Abbas, W. M. A. Wan Daud, "Hydrogen production by methane decomposition: A review," Int. J. Hydro. Energy **35**, 1160-1190 (2010).

[6] P. Tomkins, A. Mansouri, S. E. Bozbag, F. Krumeich, M. B. Park, E. M. C. Alayon, M. Ranocchiari, J. A. van Bokhoven, "Isothermal Cyclic Conversion of Methane into Methanol over Copper-Exchanged Zeolite at Low Temperature," Angew. Chem. Int. Ed. **55**, 5467-5471 (2016).

[7] Q. Zhang, D. He, Q. Zhu, "Direct partial oxidation of methane to methanol: Reaction zones and role of catalyst location," J. Nat. Gas Chem. **17**, 24-28 (2008).

[8] S. Grundner, M. A. C. Markovits, G. Li, M. Tromp, E. A. Pidko, E. J.M. Hensen, A. Jentys, M. Sanchez-Sanchez, J. A. Lercher, "Single-Site Trinuclear Copper Oxygen Clusters in Mordenite for Selective Conversion of Methane to Methanol," Nat. Commun. **6**, 7546-7555 (2015).

[9] V. L. Sushkevich, D. Palagin, M. Ranocchiari, J. A. van Bokhoven, "Selective Anaerobic Oxidation of Methane Enables Direct Synthesis of Methanol," Science **356**, 523-527 (2017).

[10] G. Li, P. Vassilev, M. Sanchez-Sanchez, J. E. J. M. Lercher, E. A. Hensen, Pidko, "Stability and Reactivity of Copper Oxo-Clusters in ZSM-5 Zeolite for Selective Methane Oxidation to Methanol," J. Catal. **338**, 305-312 (2016).

[11] P. Tomkins, M. Ranocchiari, J. A. van Bokhoven, "Direct Conversion of Methane to Methanol under Mild Conditions over Cu-Zeolites and Beyond," Acc. Chem. Res. **50**, 418-425 (2017).

[12] S. I. Chan, S. S.- F. Yu, "Controlled Oxidation of Hydrocarbons by the Membrane-Bound Methane Monooxygenase: The Case for a Tricopper Cluster," Acc. Chem. Res. **41**, 969-979 (2008).

[13] S. I. Chan, Y.-J. Lu, P. Nagababu, S. Maji, M.-C. Huang, M. M. Lee, I.-J. Hsu, P. D. Minh, J. C.-H. Lai, K. Y. Ng, S. Ramalingam, S. S.-F. Yu, M. K. Chan, "Efficient Oxidation of Methane to Methanol by Dioxygen Mediated by Tricopper Clusters," Angew. Chem., Int. Ed. **52**, 3731-3735 (2013).

[14] J. Shan, M. Li, L. F. Allard, S. Lee, M. Flytzani-Stephanopoulos, Nature **551**, 605-608 (2017**)**.

[15] A. I. Olivos-Suarez, À. Szecsenyi, E. J. M. Hensen, J. Ruiz-Martinez, E. A. Pidko, J. Gascon, "Strategies for the Direct Catalytic Valorization of Methane Using Heterogeneous Catalysis: Challenges and Opportunities," ACS Catal. **6**, 2965-2981 (2016).

[16] A. A. Latimer, A. Kakekhani, A. R. Kulkarni, J. K. Nørskov, ACS Catal. **8**, 6894-6907 (2018).

[17] K. Narsimhan, K. Iyoki, K. Dinh, Y. Roman-Leshkov, "Catalytic Oxidation of Methane into Methanol over Copper-Exchanged Zeolites with Oxygen at Low Temperature," ACS Cent. Sci. **2**, 424-429 (2016).

[18] M. Ravi, M. Ranocchiari, J. A. van Bokhoven, “The Direct Catalytic Oxidation of Methane to Methanol-A Critical Assessment”, Angew. Chem., Int. Ed. **56**, 16464-16483 (2017).

[19] Z. Zuo, P. J. Ramírez, S. D. Senanayake, P. Liu, J. A. Rodriguez, “Low-Temperature Conversion of Methane to Methanol on CeO_x/Cu_2O Catalysts: Water Controlled Activation of the C–H Bond,” J. Am. Chem. Soc. **138**, 13810-13813 (2016).

[20] D. K. Pappas, E.Borfecchia, M. Dyballa, I. A.Pankin, K. A. Lomachenko, A. Martini, M.Signorile, S. Teketel, B. Arstad, G. Berlier, C. Lamberti, S. Bordiga, U. Olsbye, K. P. Lillerud, S. Svelle, P. Beato, “Methane to Methanol: Structure–Activity Relationships for Cu-CHA,” J. Am. Chem. Soc. **139**, 14961-14975 (2017).

[21] P. Schwach, X. Pan, X. Bao, “Direct Conversion of Methane to Value-Added Chemicals over Heterogeneous Catalysts: Challenges and Prospects,” Chem. Rev. **117**, 8497-8520 (2017).

[22] R. Banerjee, Y. Proshlyakov, J. D. Lipscomb, D. A. Proshlyakov, “Structure of the key species in the enzymatic oxidation of methane to methanol,” Nature **518**, 431-434 (2015).

[23] H. V. Le, S. Parishan, A. Sagaltchik, H. Ahi, A. Trunschke, R. Schom-cker, A. Thomas, “Stepwise Methane-to-Methanol Conversion on CuO/SBA-15,” Chem. Eur. J. **24**, 12592- 12599 (2018).

[24] T. Yumura, T. Amenomori, Y. Kagawa, K. Yoshizawa, “Mechanism for the Formaldehyde to Formic Acid and the Formic Acid to Carbon Dioxide Conversions Mediated by an Iron-Oxo Species,” J. Phys. Chem. A **106**, 621-630 (2002).

[25] M. A. Nieva, M. M. Villaverde, A. Monzón, T. F. Garetto, A. J. Marchi, “Steam-methane reforming at low temperature on nickel-based catalysts,” Chem. Eng. J. **235**, 158-166 (2014).

[26] J. Liu, “Catalysis by Supported Single Metal Atoms,” ACS Catal. **7**, 34-59 (2017).

[27] S. Yang, Y. J. Tak, J. Kim, A. Soon, H. Lee, “Support Effects in Single-Atom Platinum Catalysts for Electrochemical Oxygen Reduction,” ACS Catal. **7**, 1301-1307 (2017).

[28] Y.-Q. Su, I. A. W. Filot, J.-X. Liu, E. J. M. Hensen, “Stable Pd-Doped Ceria Structure for CH_4 Activation and CO Oxidation,” ACS Catal. **8**, 75-80 (2018).

[29] P. Xie, T. Pu, A. Nie, S. Hwang, S. C. Purdy, W. Yu, D. Su, J. T. Miller, C. Wang, “Nanoceria-Supported Single-Atom Platinum Catalysts for Direct Methane Conversion,” ACS Catal. **8**, 4044-4048 (2018).

[30] M. D. Marcinkowski, M. T. Darby, J. Liu, J. M. Wimble, F. R. Lucci, S. Lee, A. Michaelides, M. Flytzani-Stephanopoulos, M. Stamatakis, E. C. H. Sykes, “Pt/Cu single-atom alloys as coke-resistant catalysts for efficient C-H activation,” Nature Chem. **10**, 325-332 (2018).

[31] R. B. Duarte, F. Krumeich, J. A. van Bokhoven, “Structure, Activity, and Stability of Atomically Dispersed Rh in Methane Steam Reforming,” ACS Catal. **4**, 1279-1286 (2014).

[32] X. Guo, G. Fang, G. Li, H. Ma, H. Fan, L. Yu, C. Ma, X. Wu, D. Deng, M. Wei, D. Tan, R. Si, S. Zhang, J. Li, L. Sun, Z. Tang, X. Pan, X. Bao, “Direct, Nonoxidative Conversion of Methane to Ethylene, Aromatics, and Hydrogen,” Science **344**, 616-619 (2014).

[33] Z. Zuo, S. Liu, Z.;Wang, C. Liu, W. Huang J. Huang, P. Liu, “Dry Reforming of Methane on Single-Site Ni/MgO Catalysts: Importance of Site Confinement,” ACS Catal. **8**, 9821-9835 (2018).

[34] J. Yuan, W. Zhang, X. Li, J. Yang, “A high performance catalyst for methane conversion to methanol: graphene supported single atom Co,” Chem. Commun. **54**, 2284-2287 (2018).

[35] J. S. Lee, S. Kim, K. H. Lee, I.-S. Nam, J. S. Chung, Y. G. Kim, H. C. Woo, “Role of alkali promoters in K/MoS_2 catalysts for CO-H_2 reactions,” Appl. Catal., A **110**, 11-25 (1994).

[36] M. Huang, K. Cho, “Density Functional Theory Study of CO Hydrogenation on a MoS_2 Surface,” J. Phys. Chem. C **113**, 5238-5243 (2009).

[37] P. Liu, Y. Choi, Y. Yang, M. G. White, “Methanol Synthesis from H_2 and CO_2 on a Mo_6S_8 Cluster: A Density Functional Study,” J. Phys. Chem. A **114**, 3888-3895 (2010).

[38] C. Liu, P. Liu, “Mechanistic Study of Methanol Synthesis from CO_2 and H_2 on a Modified Model Mo_6S_8 Cluster,” ACS Catal. **5**, 1004-1012 (2015).

[39] X. Zheng, S. Guo, L. Guo, “Ethanol synthesis catalyzed by single Ni atom supported on Mo_6S_8 support,” Appl. Catal. A: General **553**, 52-64 (2018).

[40] X. Zheng, L. Guo, W. Li, Z. Cao, N. Liu, Q. Zhang, M. Xing, Y. Shi, J. Guo, “Insight into the Mechanism of Reverse Water-gas Shift Reaction and Ethanol Formation Catalyzed by Mo_6S_8-TM Clusters,” Mol. Catal. 439, 155-162 (2017).

[41] Z. Cao, L. Guo, X. Zheng, W. Li, Y. Shi, J. Guo, Y. Xi, “Theoretical study on the reaction mechanism of reverse water–gas shift reaction using a Rh–Mo_6S_8 cluster,” RSC Adv. **2016**, 6, 108270-108279.

[42] P. E. Blöchl, “Projector Augmented-wave Method,” Phys. Rev. B **50**, 17953-17979 (1994).

[43] G. Kresse, J. Hafner, “Ab Initio Molecular Dynamics for Liquid Metals,” Phys. Rev. B **47**, 558-561 (1993).

[44] G. Kresse, J. Furthmüller, “Efficient Iterative Schemes for Ab Initio Total-energy Calculations Using a Plane-Wave Basis Set,” Phys. Rev. B **54**, 11169-11186 (1996).

[45] P. P. John, B. Kieron, E. Matthias, “Generalized Gradient Approximation Made Simple,” Phys. Rev. Lett. **77**, 3865-3968 (1996).

[46] D. Sheppard, R. Terrell, “Optimization Methods for Finding Minimum Energy Paths,” J. Chem. Phys. **128**, 134106 (2008).

[47] B. J. Berne, G. Ciccotti, D. F. Coker, “Classical and Quantum Dynamics in Condensed Phase Simulations,” Ed. World Scientific, 1998.

[48] G. Henkelman, B.P. Uberuaga, H. Jónsson, “A climbing Image Nudged Elastic Band Method for Finding Saddle Points and Minimum Energy Paths,” J. Chem. Phys. **113**, 9901-9904 (2000).

[49] G. Henkelman, H. Jónsson, “Improved Tangent Estimate in the Nudged Elastic Band Method for Finding Minimum Energy Paths and Saddle Points,” J. Chem. Phys. **113**, 9978-9985 (2000).

[50] D. Sheppard, P. Xiao, W. Chemelewski, D. D Johnson, G. Henkelman, “A Generalized Solid-State Nudged Elastic Band Method,” J. Chem. Phys. **136**, 074103 (2012).

[51] D. Sheppard, G. Henkelman, “Paths to Which the Nudged Elastic Band Converges,” J. Comp. Chem. **32**, 1769-1771 (2011).

[52] A. A. Latimer, A. R. Kulkarni, H. Aljama, J. H. Montoya, J. S. Yoo, C. Tsai, F. Abild-Pedersen, F. Studt, J. K. Nørskov, “Understanding trends in C-H bond activation in heterogeneous catalysis,” Nat Mater. **16**, 225-229 (2017).

[53] B. Hammer, J. K. Nørskov, “Theoretical surface science and catalysis-calculations and concepts,” Adv. Catal. **45**, 71-129 (2000).

[54] K. Yoshizawa, “Two-step concerted mechanism for methane hydroxylation on the diiron active site of soluble methane monooxygenase,” J. Inorg. Biochem. **78**, 23-34 (2000).

[55] K. Yoshizawa, Y. Shiota, T. Yumura, T. Yamabe, “Direct Methane-Methanol and Benzene-Phenol Conversions on Fe-ZSM-5 Zeolite: Theoretical Predictions on the Reaction Pathways and Energetics,” J. Phys. Chem. B **104**, 734-740 (2000).

[56] M. H. Mahyuddin, A. Staykov, Y. Shiota, K. Yoshizawa, “Direct Conversion of Methane to Methanol by Metal-Exchanged ZSM‑5 Zeolite (Metal = Fe, Co, Ni, Cu),” ACS Catal. **6**, 8321-8331 (2016).

[57] X.-R. Shi, S.-G. Wang, J. Hu, H. Wang, Y.-Y. Chen, Z. Qin, J. Wang, “Density Functional Theory Study on Water-Gas-Shift Reaction over Molybdenum Disulfide,” Appl. Catal. A: General **365**, 62-70 (2009).

[58] F. Göltl, C. Michel, P. C. Andrikopoulos, A. M. Love, J. Hafner, I. Hermans, P. Sautet, “Computationally Exploring Confinement Effects in the Methane-to-Methanol Conversion Over Iron-Oxo Centers in Zeolites,”ACS Catal. **6**, 8404-8409 (2016).

[59] S. Ye, C.-Y. Geng, S. Shaik, F. Neese, “Electronic structure analysis of multistate reactivity in transition metal catalyzed reactions: the case of C–H bond activation by non-heme iron(IV)–oxo cores,” Phys. Chem. Chem. Phys. **15**, 8017-8030 (2013).

Table 1. Adsorption energy (eV) of single-metal-atom, M, over Mo_6S_8 cluster.

M	K	Ti	Fe	Co	Ni	Cu	Rh
E_{ads}	-2.71	-5.24	-3.77	-3.57	-3.69	-2.55	-4.33

Table 2. Adsorption energy (eV) of molecule CH_4 on bare and single-metal-atom modified Mo_6S_8 clusters.

Site	Mo_6S_8	K-Mo_6S_8	Ti-Mo_6S_8	Fe-Mo_6S_8	Co-Mo_6S_8	Ni-Mo_6S_8	Cu-Mo_6S_8	Rh-Mo_6S_8
Mo	-0.30	-0.17	-0.21	-0.10	-0.15	-0.13	-0.18	-0.12
M		-0.11	-0.46	-0.36	-0.48	-0.53	-0.38	-0.05

Table 3. Adsorption energy (eV) of molecule H_2O on bare and single-metal-atom modified Mo_6S_8 clusters.

Site	Mo_6S_8	K-Mo_6S_8	Ti-Mo_6S_8	Fe-Mo_6S_8	Co-Mo_6S_8	Ni-Mo_6S_8	Cu-Mo_6S_8	Rh-Mo_6S_8
Mo	-0.83	-0.88	-0.78	-0.75	-0.79	-0.75	-0.80	-0.80
M		-0.52	-1.02	-0.92	-0.99	-0.97	-0.88	-0.79

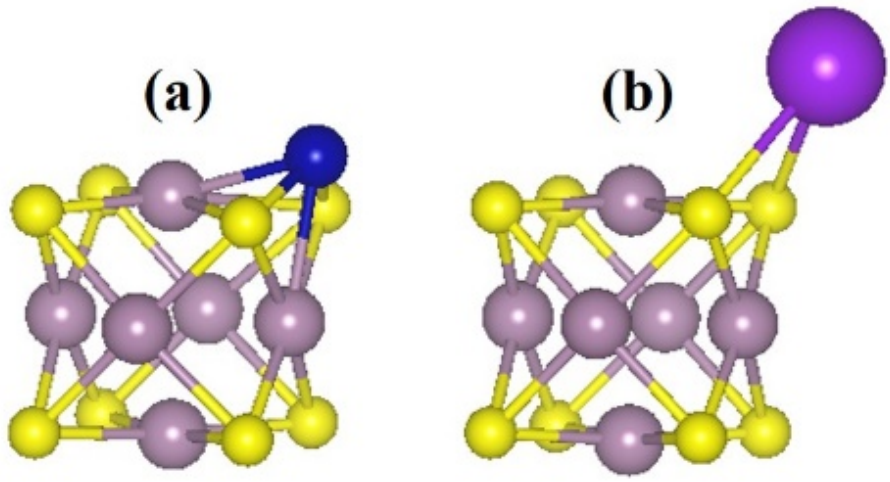

Figure 1. Optimized M-Mo_6S_8 structure. (a) M atom anchored at S-Mo-Mo-S 4-fold site; (b) M atom anchored at S-S 2-fold site. (Mo: small purple, S: yellow, M: big purple or dark blue.)

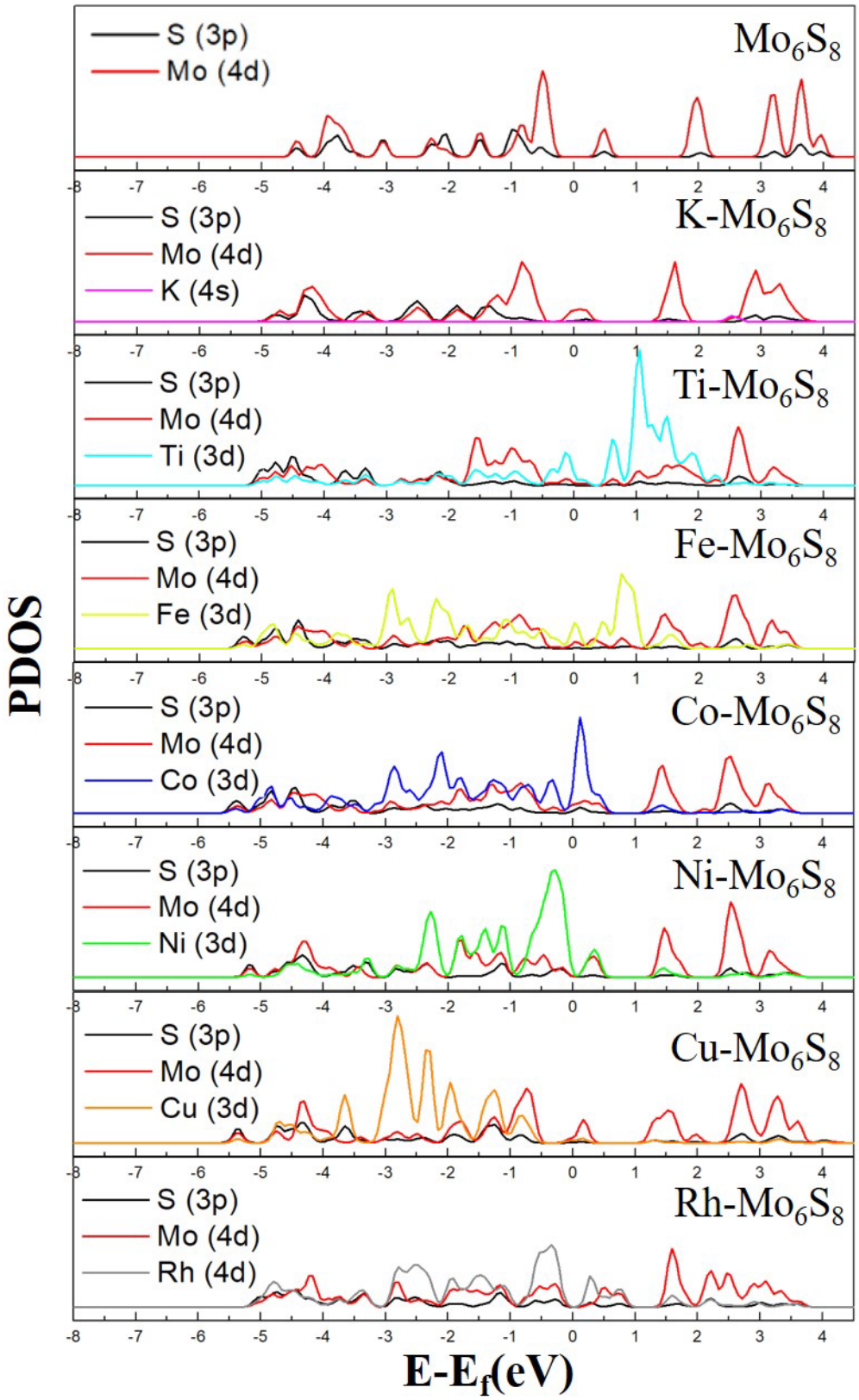

Figure 2. Partial density of states of Mo_6S_8 and metal modified M-Mo_6S_8 (M = K, Ti, Fe, Co, Ni, Cu, and Rh) cluster.

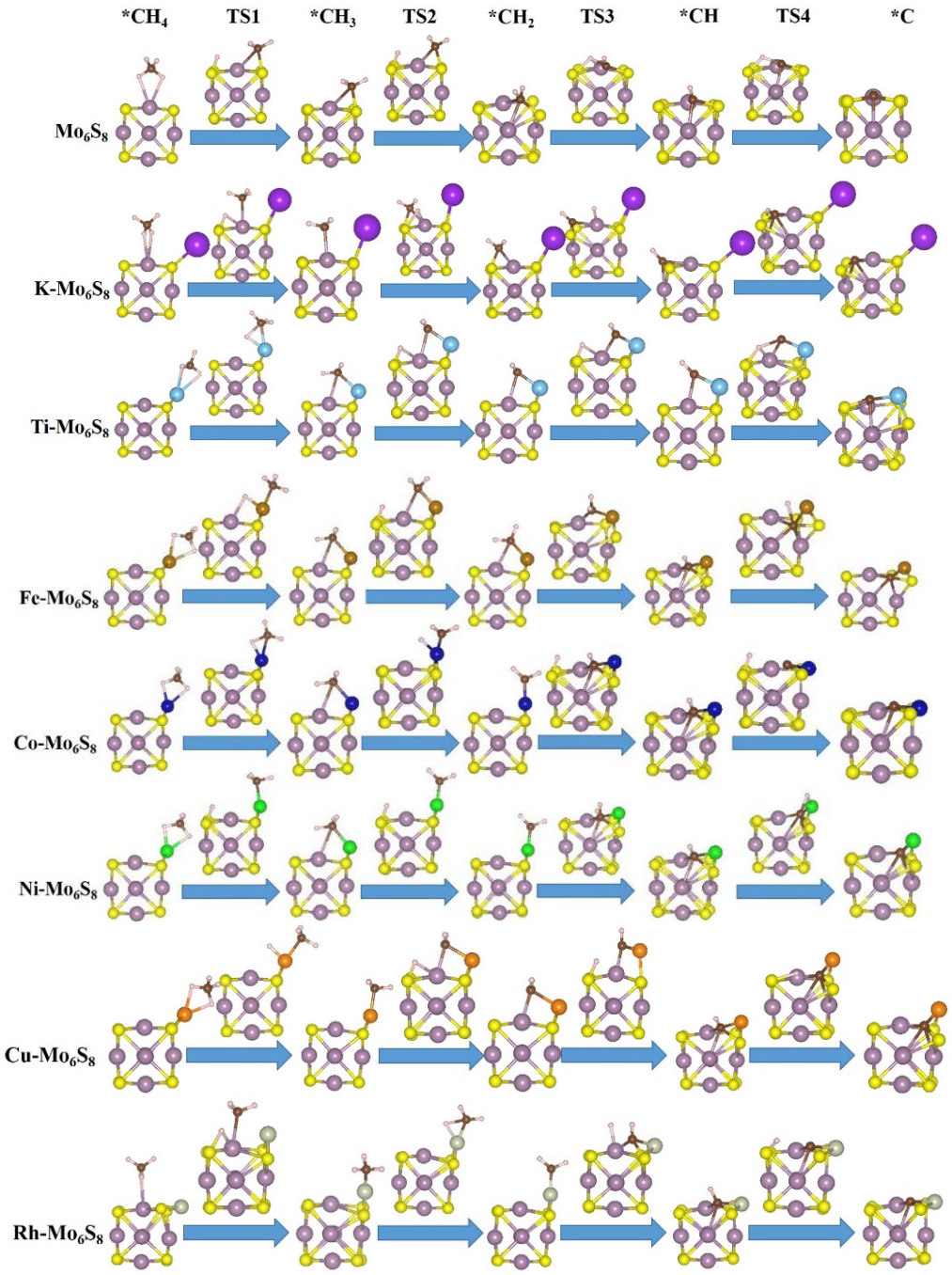

Figure 3. Geometries of the reaction intermediates and transition states (TS) involved in CH_4 dissociation on single-metal-atom modified Mo_6S_8 clusters (Mo: small purple, S: yellow, C: brown, H: white, metal: K-big purple, Ti-light blue, Fe-wine, Co-dark blue, Ni-green, Cu-orange, Rh-grey).

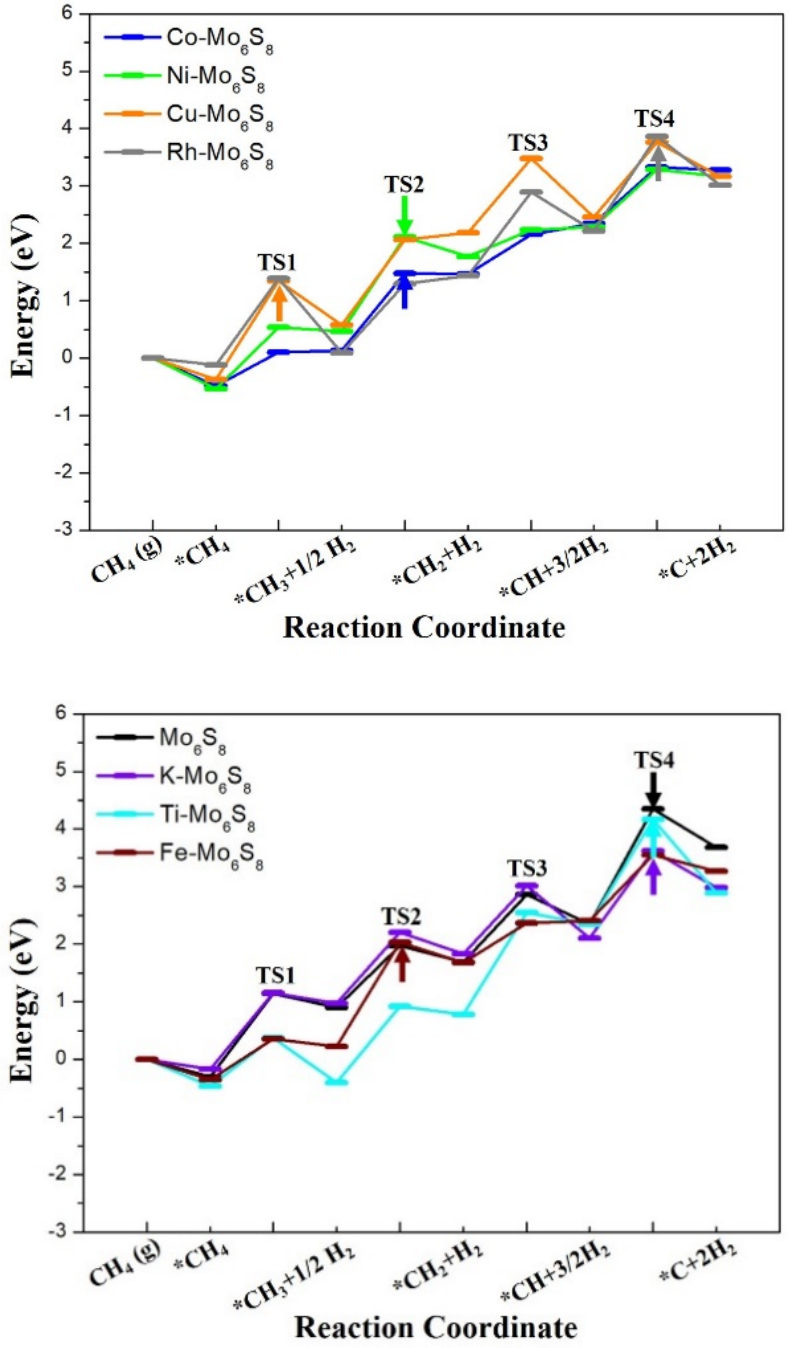

Figure 4. Optimal Potential Energy Diagrams for CH_4 dissociation on bare, K-, Ti-, and Fe-Mo_6S_8 cluster (top) and Co-, Ni-, Cu-, and Rh-Mo_6S_8 cluster (bottom). Arrows point to the steps with highest barrier.

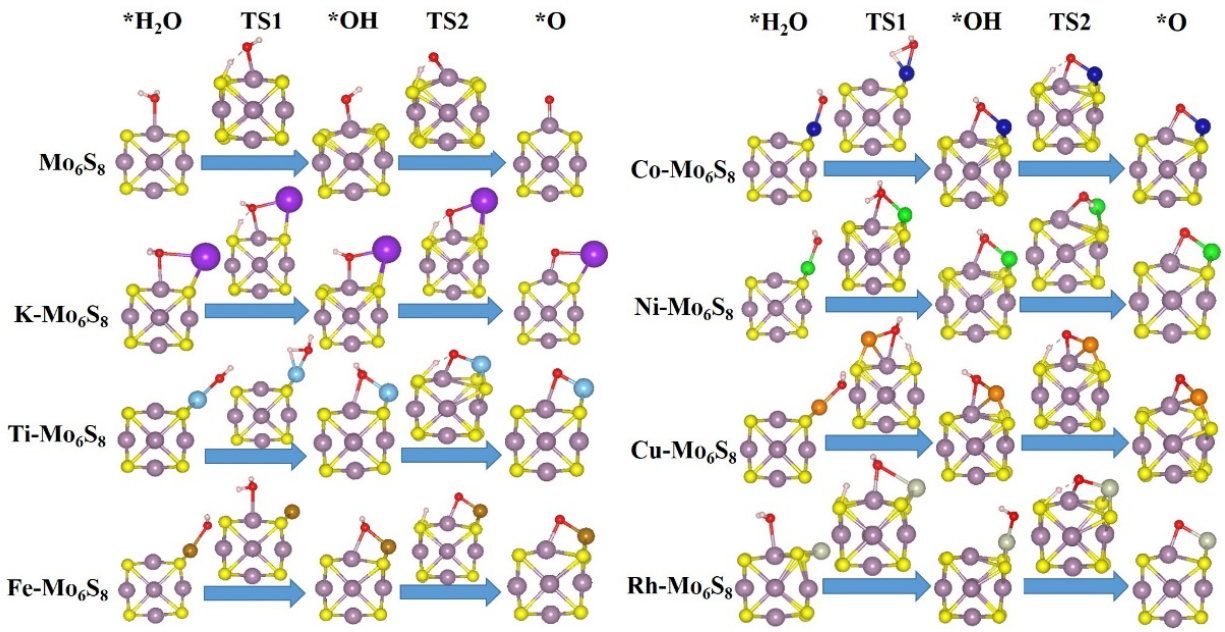

Figure 5. Geometries of the reaction intermediates and transition states (TS) involved in H_2O dissociation on single-metal-atom modified Mo_6S_8 clusters (Mo: small purple, S: yellow, C: brown, H: white, metal: Co-dark blue, K-big purple, Ni-green, Ti-light blue, Cu-orange, Fe-wine, Rh-grey)

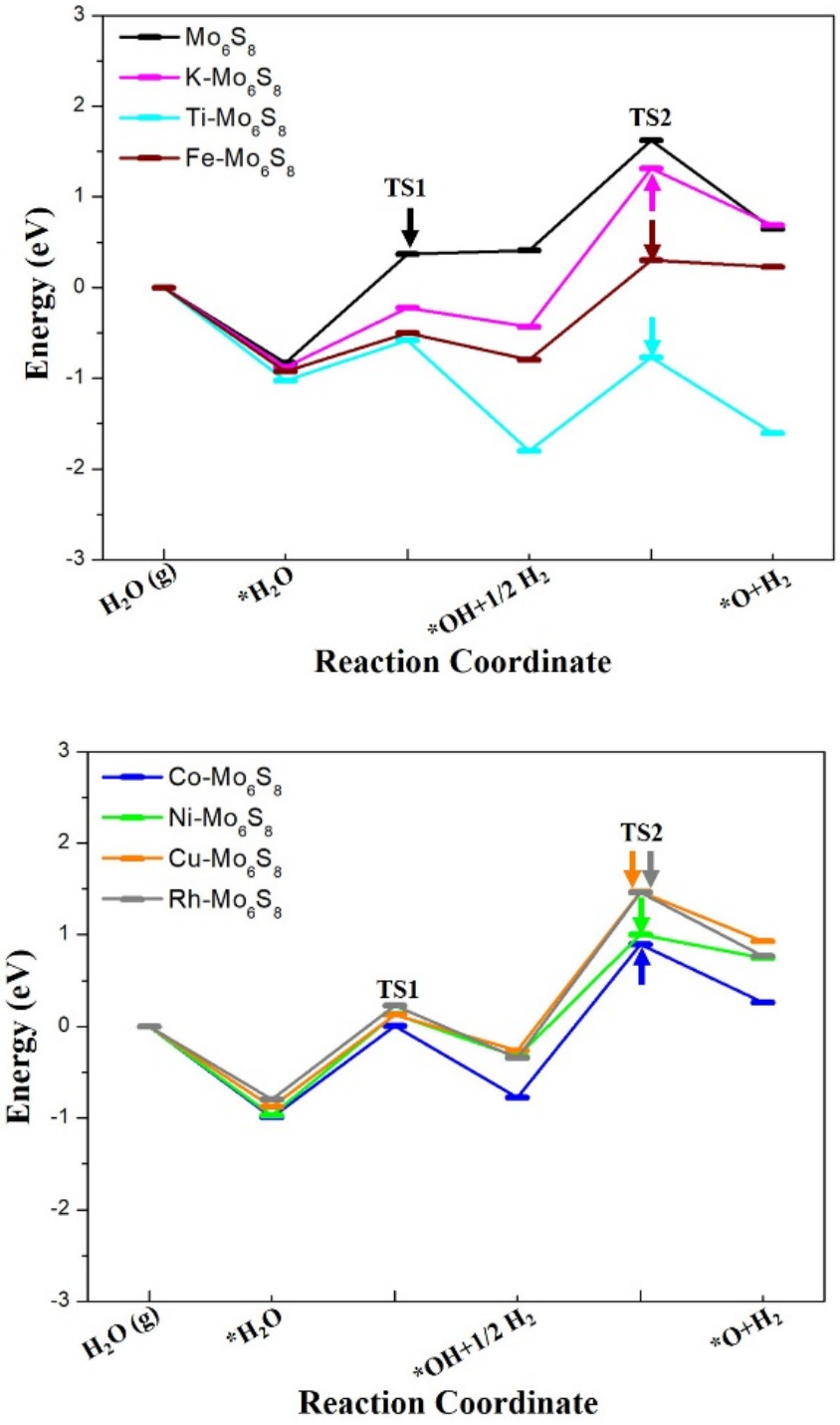

Figure 6. Optimal Potential Energy Diagrams for H_2O dissociation on bare, K-, Ti-, and Fe-Mo_6S_8 cluster (top) and Co-, Ni-, Cu-, and Rh-Mo_6S_8 cluster (bottom). Arrows point to the steps with highest barriers.

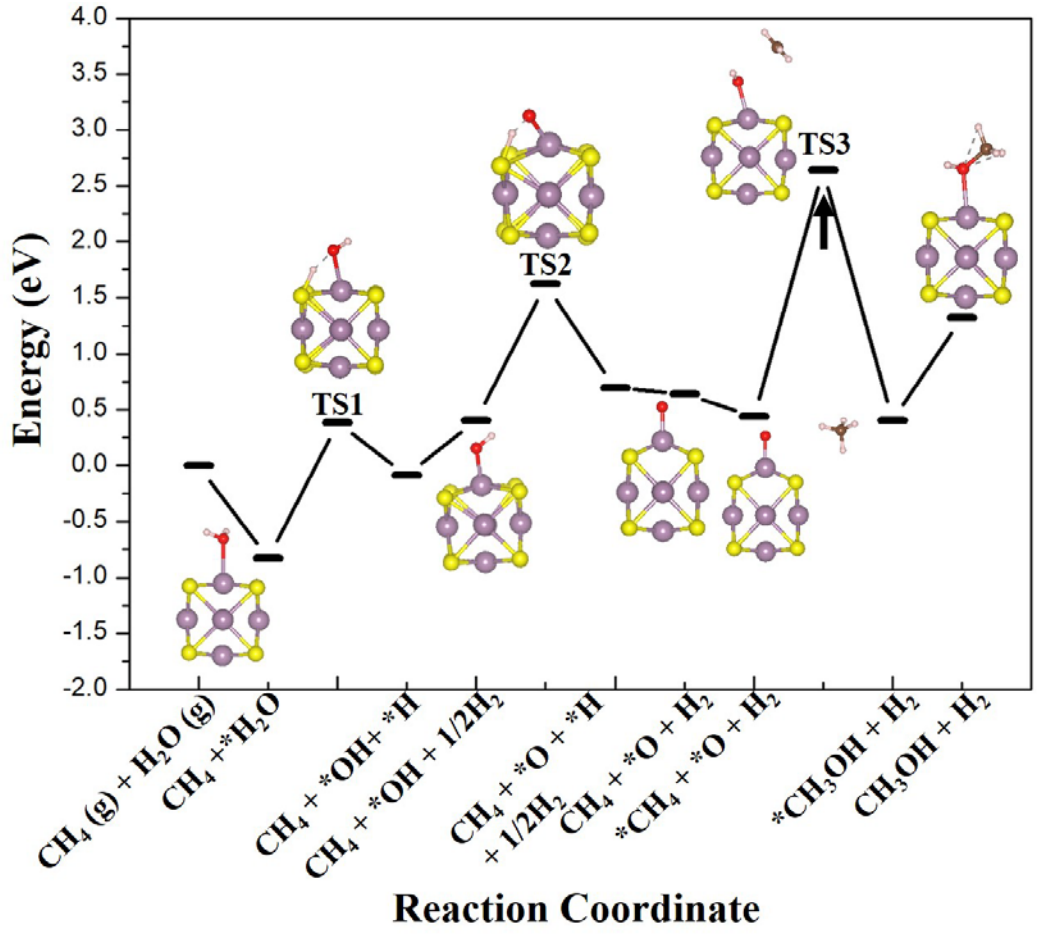

Figure 7. Optimal potential energy diagram and geometries of intermediates and transition states (TS) for the SRM to CH_3OH synthesis on the Mo_6S_8 cluster. The arrow pointes to the step with the highest energy barrier. (Mo: small purple, S: yellow, C: brown, H: white, O: red)

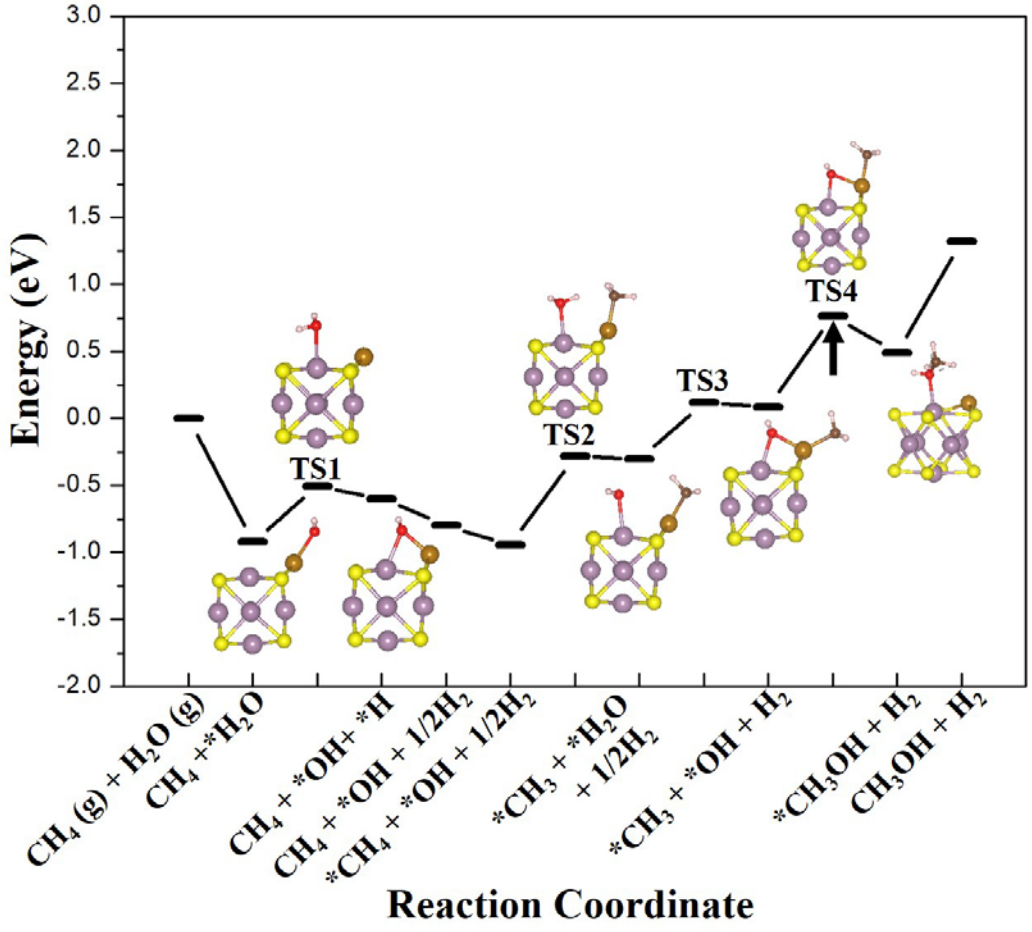

Figure 8. Optimal potential energy diagram and geometries intermediates and transition states (TS) for CH_3OH synthesis on Fe-Mo_6S_8 cluster. The arrow pointes to the step with the highest energy barrier. (Mo: small purple, S: yellow, C: brown, H: white, O: red, Fe: wine)

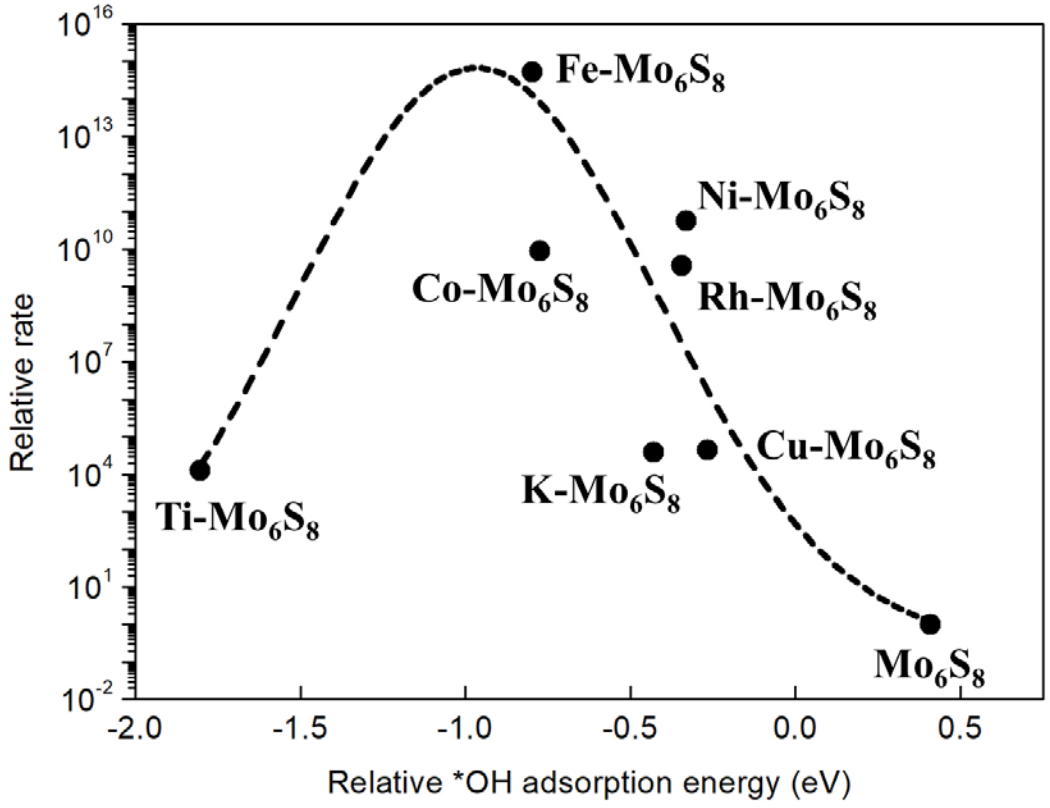

Figure 9. The variation in relative rate for the SRM to CH_3OH over M-Mo_6S_8 clusters with the corresponding *OH adsorption energy.